# *Studies on Diels–Alder thermoresponsive networks based on ether–urethane bismaleimide functionalized poly(vinyl alcohol)*

**Oana Ursache, Constantin Gaina, Viorica Gaina, Nita Tudorachi, Alexandra Bargan, Cristian-Dragos Varganici & Dan Rosu**

**Journal of Thermal Analysis and Calorimetry**
An International Forum for Thermal Studies

ISSN 1388-6150
Volume 118
Number 3

J Therm Anal Calorim (2014)
118:1471-1481
DOI 10.1007/s10973-014-4041-7

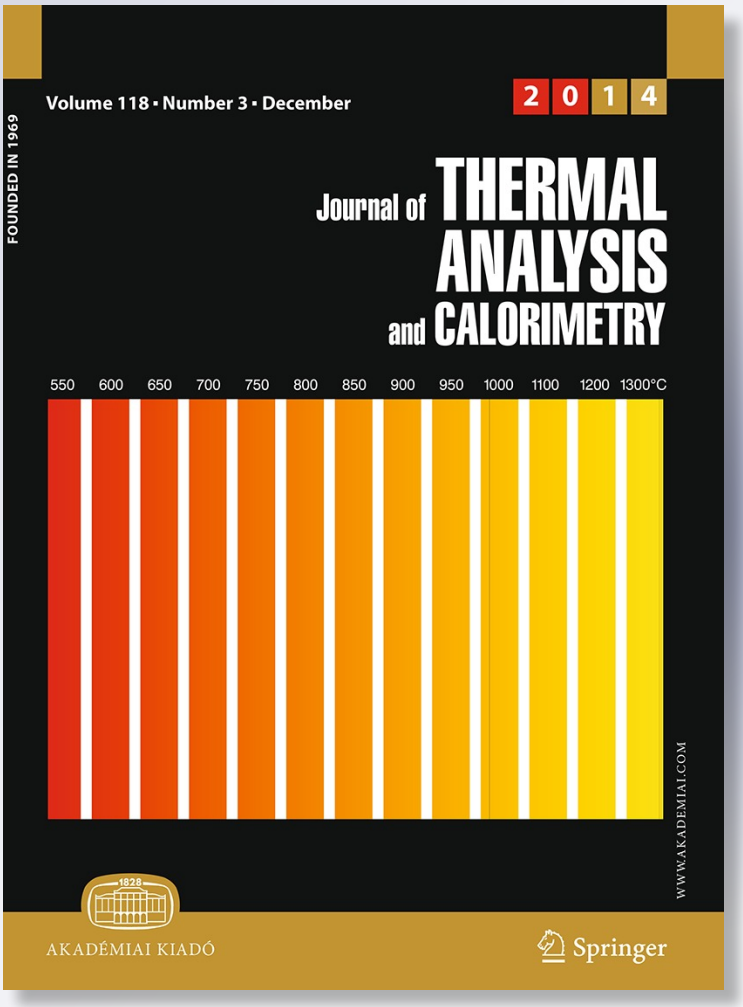


Springer

J Therm Anal Calorim (2014) 118:1471–1481
DOI 10.1007/s10973-014-4041-7

# Studies on Diels–Alder thermoresponsive networks based on ether–urethane bismaleimide functionalized poly(vinyl alcohol)

**Oana Ursache · Constantin Gaina · Viorica Gaina · Nita Tudorachi · Alexandra Bargan · Cristian-Dragos Varganici · Dan Rosu**

Received: 4 April 2014 / Accepted: 16 July 2014 / Published online: 26 August 2014


**Abstract** Thermoreversible networks obtained by the Diels–Alder cycloaddition reaction of poly(vinyl furfural) with urethane bismaleimides containing polyether chain were synthesized. The formation of the networks was confirmed by attenuated total reflectance in conjunction with Fourier transform infrared spectroscopy (ATR–FTIR). The materials thermal properties were investigated using differential scanning calorimetry (DSC) and a coupling of dynamic thermogravimetry with Fourier transform infrared spectroscopy and mass spectrometry (TG–FTIR–MS) for pyrolysis behaviour under nitrogen atmosphere. A thermal decomposition mechanism of the networks and poly(vinyl furfural) was discussed via evolved gas analysis. The thermoreversibility of the networks was demonstrated by the presence of the endothermic peak characteristic to the retrodienic process on the DSC heating curves and also the appearance of the exothermic peak, due to the dienic process, on the DSC cooling curve. The dynamic contact angle and free surface energy values of the networks were determined. Measures of the heterogeneity and roughness of the surfaces suggested that the surfaces of the networks' films are more homogenous than the initial poly(vinyl furfural) surface. Dynamic water vapour sorption studies were conducted.

**Keywords** Retro-Diels–Alder · Thermal properties · Pyrolysis behaviour · Evolved gas analysis · Contact angle · Water vapour sorption

## Introduction

Poly(vinyl alcohol) (PVA), a water soluble polymer satisfied requirements in fields such as packaging and pharmacy. An advantage of PVA consists in the fact that it is a biodegradable polymer with hydroxyl functionality. Its main disadvantages are the low antimicrobial activity, mechanical and thermal stability [1]. In order to improve these properties, the structure of PVA needed modified. The research and development of novel soft materials that possess unique properties enabled enormous opportunities in the fields of nanotechnology, biotechnology and medicine. Structural modification of PVA can be made with monofunctional and bifunctional compounds, the bifunctional ones leading to the crosslinking of PVA [2–5], whereas the monofunctional to simple chemical change to the hydroxyl groups of PVA without any crosslinking [6–12].

Cycloaddition reaction of poly(vinyl furfural) (PVF), obtained by acetalisation of PVA with 2-furfural, with bismaleimide leads to the obtaining of thermoreversible crosslinked networks [13]. Recently the Diels–Alder (DA) reaction based on macromolecular chemistry has attracted

Paper dedicated to the 65th anniversary of ''Petru Poni'' Institute of Macromolecular Chemistry of Romanian Academy, Iasi, Romania.

O. Ursache · C. Gaina · V. Gaina
Laboratory of Polyaddition and Photochemistry, "Petru Poni" Institute of Macromolecular Chemistry, 41A Gr. Ghica-Voda Alley, 700487 Iasi, Romania

N. Tudorachi · A. Bargan
Inorganic Polymers Department, "Petru Poni" Institute of Macromolecular Chemistry, 41A Gr. Ghica-Voda Alley, 700487 Iasi, Romania

C.-D. Varganici (✉) · D. Rosu
Centre of Advanced Research in Bionanoconjugates and Biopolymers, "Petru Poni" Institute of Macromolecular Chemistry, 41A Gr. Ghica-Voda Alley, 700487 Iasi, Romania
e-mail: varganici.cristian@icmpp.ro; varganicicristian@yahoo.com

much attention particularly for providing new materials [14–19]. The thermoreversibility of the DA reaction is an interesting feature. The DA reaction between a diene and a dienophile forms covalent bonds which can be easily cleaved on heating. The equilibrium of the DA reaction could be displaced towards the reagents by heating through the retro-DA (rDA) reaction [20–27]. The utilization of the DA reaction in polymer crosslinking to build up polymer networks results in a new class of thermally reversible crosslinked polymers. In recent years, these thermally reversible crosslinked polymers were widely studied to explore applications in hydrogels [28, 29], encapsulants [30], adhesives [31], coatings [26] and structural materials with shape-memory [32, 33].

Another interesting application of this reaction in polymers is the formation of thermally reversible networks. Due to the reversible nature of the reaction, it might be possible to control the molecular mass of polymers and therefore, some thermal and mechanical properties. Polymers bearing pendant diene or dienophile groups have been crosslinked by reaction with a bisdienophile or a bisdiene, respectively [34–36]. Thus, thermoreversible networks have been prepared using copolymers functionalized with furylic groups [34–36], polyamides with maleimidic functional groups [37, 38], polyurethanes functionalized with furylic groups [39] or maleimide [40–42], PVF [13].

In a previous paper, some thermoreversible networks based on PVF and maleimide multifunctional monomers were synthesized [13]. However, due to the rigidity of these networks and consequently to the high glass transition temperatures, the retrodienic process was delayed and overlapped with the glass transition.

The purpose of this investigation is to study the influence of the acetalisation degree of PVF and molecular mass of urethane bismaleimide on the thermal properties using differential scanning calorimetry (DSC) and the pyrolysis behaviour by thermogravimetry coupled with Fourier transform infrared spectroscopy and mass spectrometry (TG–FTIR–MS). The dynamic water vapour sorption of the synthesized polymeric network structures was also studied. The materials may be suitable as future membranes for pervaporation of organic–water mixtures.

## Materials and methods

### Materials

PVA in white crystalline form (viscosity-average molecular mass 77,000–79,000 containing 2 % acetate groups), 2-furaldehyde 99 %, dimethylformamide (DMF), *p*-toluene sulphonic acid (*p*-TSA), poly(tetramethylene ether)glycol (PTMEG) (Terathane 250, 650, 1,000 and 2,000) were purchased from Aldrich and used as received. PVF was prepared by acetalisation of PVA in DMSO as solvent and in the presence of *p*-TSA according to a method described in the literature [29]. The urethane bismaleimides, BMI-(1–4), were prepared by the addition reaction of 4-maleimidophenyl isocyanate with PTMEG having number-average molecular masses of 250, 650, 1,000 and 2,000 according to the method described in the literature [30].

### Synthesis of crosslinked PVF–urethane BMI networks (NPVF)

To a solution of PVF (1 g) dissolved in 10 mL DMF was added BMI (2.05:1 mol) and dissolved by stirring and heating at 80 °C for 3 h. The reaction solution was degassed in vacuum and quickly transferred to a glass plate using a doctor blade (depth = 1 mm). The solvent was evaporated at 80–90 °C for 24 h. The film was removed from the glass plates by soaking in cold water.

### Methods

#### *ATR–FTIR*

The Fourier transform infrared (FTIR) spectra were recorded on a Vertex 70 (Bruker-Austria) instrument equipped with a Golden Gate single reflection ATR accessory, spectrum range 600–4,000 $cm^{-1}$.

#### *DSC*

Differential scanning calorimetry (DSC) measurements were conducted on a DSC 200 F3 Maia (Netzsch-Germany). About 9 mg of each sample was heated in pressed and pierced aluminium crucibles at a heating rate of 10 °C $min^{-1}$. Nitrogen was used as inert atmosphere at a flow rate of 50 mL $min^{-1}$.

#### *Thermal decomposition and evolved gas analysis studies*

Thermal degradation of polymers and evolved gas analysis (EGA) were performed using an online TG–DSC–FTIR–MS system. The system is equipped with an apparatus for simultaneous thermogravimetric and differential scanning calorimetry analysis, model STA 449F1 Jupiter (Netzsch-Germany), a FTIR spectrophotometer, Vertex-70 model (Bruker-Germany) and a mass spectrometer (MS) model QMS 403C, Aëolos (Netzsch-Germany). The thermogravimetric analyzer was calibrated for temperature and sensitivity using the melting points of the standard metals (Hg, In, Sn, Bi, Zn) from −38.5 to 600 °C. Sample masses ranging from 7 to 10 mg were heated from 25 to 600 °C, at

a heating rate of 10 °C $min^{-1}$. Nitrogen (99.999 % purity) was used as carrier gas at a flow rate of 50 mL $min^{-1}$ and as a protective purge gas for the thermobalance at a flow rate of 20 mL $min^{-1}$. The samples were heated in open $Al_2O_3$ crucibles, and another identical empty crucible was used as reference material. Data collection was carried out with Proteus software version 5.2 supplied by Netzsch. The gases released during thermal decomposition were transferred through an isothermal transition line to the FTIR device. The FTIR transferring line is made of polytetrafluorethylene (PTFE), is 1 m long, has an interior diameter of 1.5 mm and was heated to 290 °C. A capillary quartz transfer line with 75 μm diameter, heated at 290 °C, connected the thermobalance with the QMS device. Recording of mass spectra was made under the electron impact ionization energy of 70 eV. Data were scanned in the *m/z* range from 1 to 140, and the measuring time for each cycle was 1.03 s. The gases were introduced into the TG-IR external module, and FTIR spectra were recorded in the 600–4,000 $cm^{-1}$ domain with a resolution of 4 $cm^{-1}$. The TG-IR module is equipped with a low volume gas cell ($V = 8.7$ mL), 123 mm length, heated at 290 °C to avoid the condensation of the compounds with reduced volatility, and a sensitive liquid–nitrogen cooled MCT detector (Mercury Cadmium Telluride) which covers a spectral range between 600 and 4,000 $cm^{-1}$. The acquisition of the FTIR spectra was done with OPUS 6.5 software that controls the starting and synchronizing of the apparatus.

### *Dynamic contact angles studies*

Dynamic contact angles were performed by the Wilhelmy plate technique, using a Sigma 700 precision tensiometer produced by KSV Instruments. The sample plate dimensions were 50 × 8 mm, and rate of immersion–emersion was 5 mm $min^{-1}$ in water. Immersion depth was 5 mm in standard conditions. All measurements were the average of three contact angle measurements of the samples. Also, the Wilhelmy plate method uses the interaction of a platinum plate with the surface being tested. This is a method for determination of the surface tension.

### *Dynamic water vapour sorption studies*

Dynamic water vapour sorption capacity for all the synthesized samples has been determined using the fully automated gravimetric analyzer IGAsorp produced by Hiden Analytical, Warrington (UK). It has an ultrasensitive microbalance which measures the mass change as the humidity is modified in the sample chamber at a constant regulated temperature. The system is fully automated and controlled by a software package.

## Results and discussion

### Synthesis and characterization of the crosslinked PVF–urethane BMI networks (NPVF)

The thermoreversible networks were prepared by the DA reaction of PVF having an acetalisation degree of 23 (PVF-1), 28 (PVF-2) and 30 % (PVF-3), respectively, with urethane bismaleimide BMI-(1–4) containing a PTMEG chain of different molecular masses according to Scheme 1 and Table 1.

The formation of the networks has been confirmed by the ATR–FTIR spectroscopy. For exemplification, the spectra of the networks obtained from the PVF-2 are represented in Fig. 1.

Comparing the spectra of the networks with the one of PVF-2, one can observe the disappearance or decreasing in intensity of the absorption bands at 750 and 1,004 $cm^{-1}$, bands which are characteristic to the monosubstituted furan ring and furan ring vibrations, respectively. This fact clearly indicates that the reaction occured successfully. Also, the formation of the networks is confirmed by the appearance in their spectra of an absorption band as a shoulder at 1,778 $cm^{-1}$, band which is characteristic to the furan–maleimide cycloadduct. Since there are no major structural differences between the networks, they differ only by the molecular mass number of PTMEG from the BMI structure used in the synthesis, and the only differences between their spectra are in the intensities of the absorption bands attributed to the ether linkage (which appears at about 1,100 $cm^{-1}$) and to the methylene group (appearing between 2,680 and 3,010 $cm^{-1}$), respectively, intensities which are expected to increase with PTMEG molecular mass number increase.

### Thermal properties by DSC

Using the DSC method, the influence of the molecular mass number of PTMEG on the glass transition temperature ($T_g$) and on the temperature of the endothermic peak characteristic to the retrodienic process was studied. Thus, in the DSC curves of the networks (Fig. 2), there can be observed a decrease of the $T_g$ of the network, when increasing the molecular mass of PTMEG from the BMI structure. Also, the temperature at which the retrodienic process begins, starts decreasing when increasing the molecular mass of PTMEG.

A possible explanation for the decreasing of the temperature of the retrodienic process could be the following: a higher molecular mass of PTMEG involves longer PTMEG segments and a greater distance between the PVF chains, thus leading to a higher mobility of the molecular chains. Due to the higher mobility of the chains and to the lower

**Scheme 1** Synthesis of the crosslinked PVF–urethane BMI networks

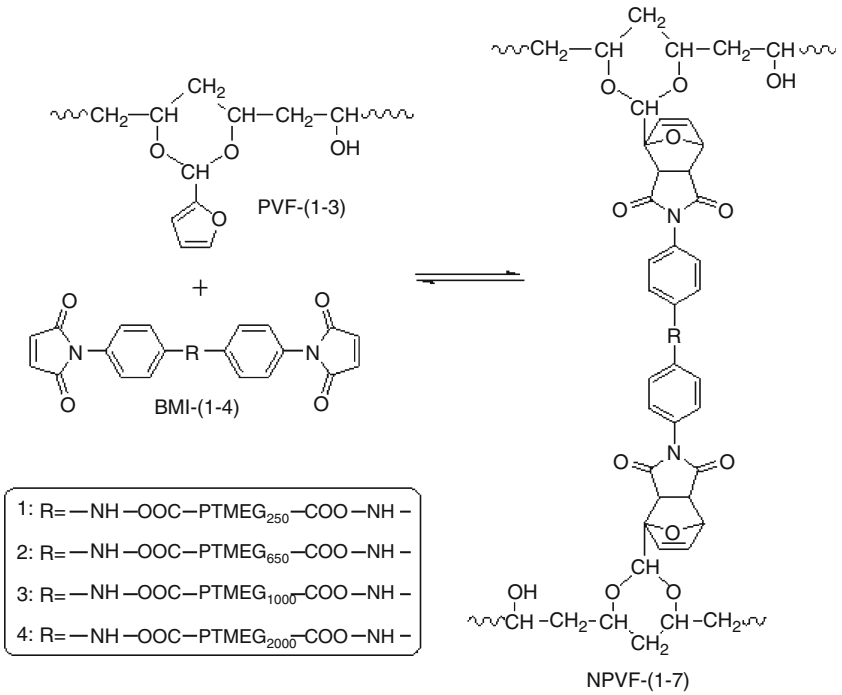


**Table 1** The composition of the networks

| Sample | PVF | BMI |
|---|---|---|
| NPVF-1 | 1 | 2 |
| NPVF-2 | 1 | 4 |
| NPVF-3 | 2 | 1 |
| NPVF-4 | 2 | 2 |
| NPVF-5 | 2 | 3 |
| NPVF-6 | 2 | 4 |
| NPVF-7 | 3 | 2 |

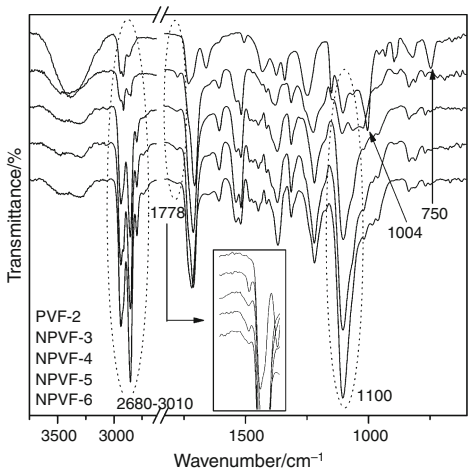


**Fig. 1** ATR–FTIR spectra of the studied structures

packing of the chain segments, the heat transfer to the cycloadducts could be faster accomplished, at a lower temperature in order for the retrodienic process to occur. The area of the endothermic peak attributed to the retrodienic reaction decreases with increasing of the molecular mass of PTMEG since the furan–maleimide cycloadduct ratio in the polymeric network is lower.

In order to observe the influence of the acetalisation degree of PVF on the $T_g$ and on the temperature of the endothermic peak characteristic to the rDA reaction, the DSC curves of the network based on BMI-2 with different acetalisation degrees were recorded (Fig. 3).

The $T_g$ value increases with the acetalisation degree of PVF increase. This behaviour is due to the increasing of the acetalisation degree of PVF which leads to an increasing of the crosslinking degree of the corresponding network, conferring a higher rigidity to the structure. The higher rigidity determines a higher $T_g$ of the network. The retrodienic process begins at a higher temperature in the case of the network based on the PVF with the highest acetalisation degree.

## Thermal stability studies

Figure 4a shows the simultaneous TG/DSC/DTG/Gram Schmidt curves for PVF-1.

It was observed from the literature that PVF-1 follows a somewhat similar thermal decomposition trend to that of poly(vinyl alcohol) [43, 44]. Analysing the DTG curves, three stages of structural thermal decomposition may be

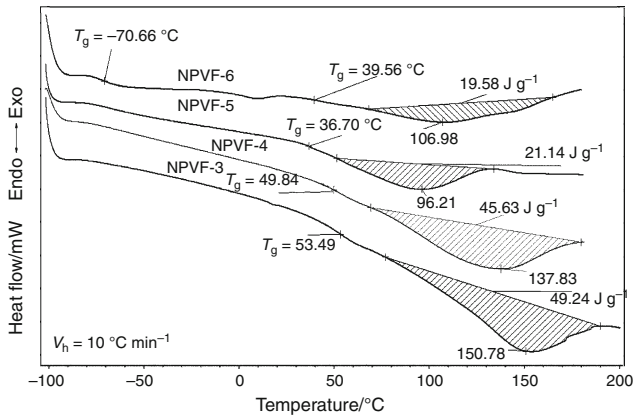


**Fig. 2** DSC curves of the studied structures

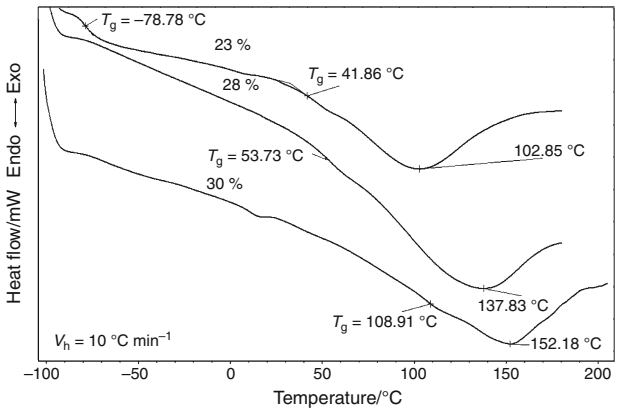


**Fig. 3** DSC curves of the network based on BMI-2 with different acetalisation degrees

observed in the case of PVF-1. First, the sample PVF-1 loses up to 2 % mass in the range 75–110 °C attributed to physical dehydration. The first thermal decomposition stage occurs in the range 200–290 °C with a mass loss of 22 % and may be attributed to the breakdown of the polymer backbone by partial dehydration with polyene formation, which further decompose in the second stage together with macroradicals cleavage. The second stage of thermal decomposition occurs in the range 300–390 °C accompanied by a mass loss of 28 %. The last stage of thermal degradation takes place in the range 390–500 °C, is accompanied by a mass loss of 37 %, and is attributed to a complex degradation of polymer chains by random cleavage reactions. A residue of 9 % was left at 600 °C. The Gram Schmidt curve shows that the highest concentrations of evolved gaseous mixtures are recorded at temperature values of 244, 334 and 441 °C, which correspond to the temperature values of the DTG curve peaks, where the thermal decomposition rates values are the highest. The three thermal decomposition stages were endothermic processes, as evidenced by the simultaneous DSC curves. Figure 4b shows the simultaneous TG/DTG/Gram Schmidt curves for NPVF-2, as an exemplification, due to the other networks similar thermal behaviour. All networks exhibited two stages of thermal decomposition. The first stage of thermal degradation of NPVF-2 ranges between 290 and 380 °C with a mass loss of 22 % and is attributed to the decomposition of mainly urethane bonds and chemical dehydration [45], while the second stage ranges between 390 and 490 °C, it is the main one and presents a 63 % mass loss attributed to the further complex and advanced structural cleavage, including ether moieties formation and decomposition of other structural entities such as furan derivatives [46]. A 13 % residue mass was found at 600 °C. All networks exhibited a seemingly higher thermal stability compared to PVF-1. It was observed that the thermal stability of the networks increased with the PTMEG molecular mass,

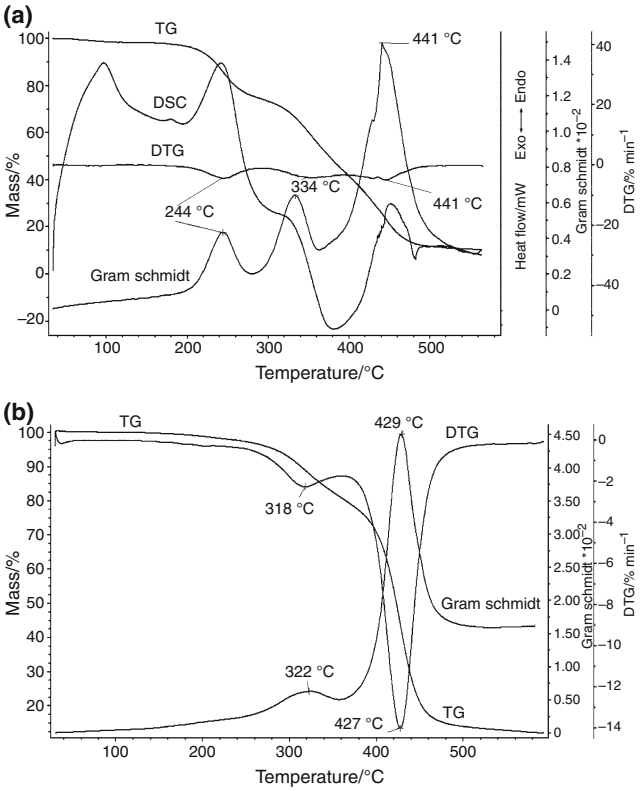


**Fig. 4** Simultaneous TG/DSC/DTG/Gram Schmidt curves for PVF–1 (**a**) and TG/DTG/Gram Schmidt curves for NPVF–2 (**b**)

since the networks last decomposition stage is also based on the oligoether chains scission. In this sense, as an example, for NPVF-2 there was a much higher mass loss than for NPVF-1 due to the much longer PTMEG chains (Fig. 5). The two thermal decomposition stages were both correlated with endothermic processes on the simultaneous recorded DSC curves (not shown here). The Gram Schmidt curve shows

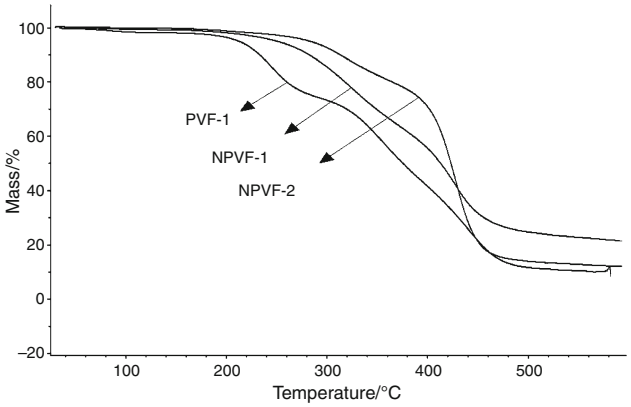


**Fig. 5** TG curves of PVF-1, NPVF-1 and NPVF-2

that the highest concentrations of evolved gaseous mixtures are recorded at temperature values of 322 and 429 °C.

## EGA studies

### *MS analysis of the evolved gases*

The interpretations of mass spectra were made in correlation with NIST Mass Spectral Database. MS spectra showed evolvement of complex gaseous mixtures. Figure 6 shows the MS spectra of the main gases evolved during thermal decomposition of PVF-1 (Fig. 6a) and NPVF-2 (Fig. 6b) and correspond to the first peaks of the Gram Schmidt curves, i.e. the first stage of thermal decomposition for each of the two samples, the other stages containing similar signals. The same aspect concerns the FTIR spectra in Fig. 7.

For PVF-1 (Fig. 6a), the *m/z* values of 18, 17 and 16 correspond to chemical dehydration. The *m/z* values of 96, 95, 67, 39, 38 and 29 were attributed to furan derivatives such as 2-furfural, continuously evolved in the temperature range 175–564 °C. In the same temperature range, the *m/z* values of 78, 52, 51, 50, 39 and 38 may correspond to some unsaturated polyene structures such as 1,5-hexadien-3-yne. Also, the signals at $m/z = 68, 67, 53, 42, 41, 39, 38$ may correspond to furan and/or some conjugated diene structures such as 1,3–pentadiene, 2-methyl-1,3-butadiene. The *m/z* values of 60, 45 and 43 correspond to acetic acid which evolved continuously in the temperature range 190–534 °C. The *m/z* values of 44, 16, 12 may be attributed to carbon dioxide evolvement continuously in the temperature range 190–414 °C. Also, the *m/z* values of 32 and 16 may be attributed to oxygen evolvement. The *m/z* values of 28, 27, 26 may correspond to ethylene evolvement in the range 205–294 °C. Ethylene oxide may be also identified in the gaseous mixture at *m/z* values of 44, 43, 42, 15 and

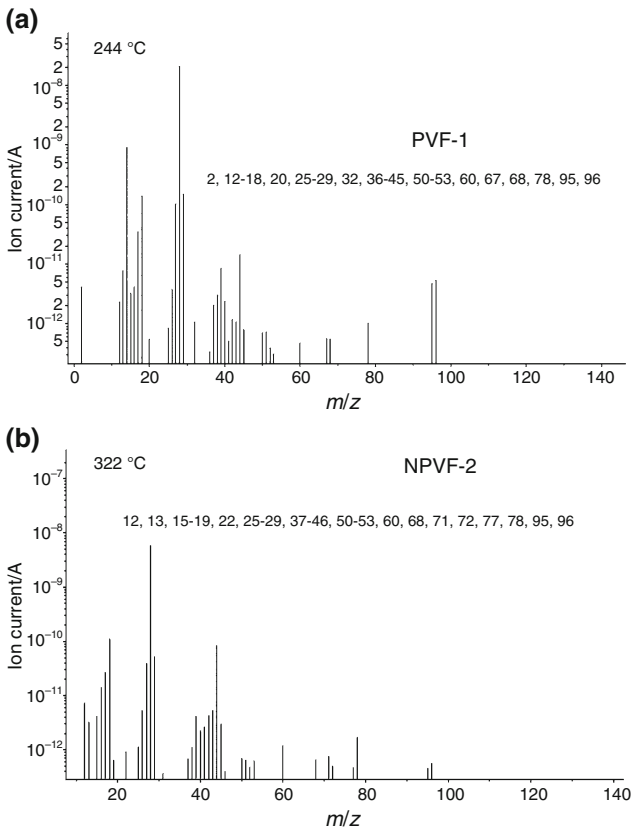


**Fig. 6** MS spectra of the gases evolved during the first stage of thermal decomposition of **a** PVF-1 and **b** NPVF-2

12 continuously evolved in the range 190–534 °C. The MS spectrum of the NPVF-2 network (Fig. 6b) exhibited all the above mentioned *m/z* signals from the thermal decomposition of PVF-1 and also new *m/z* signal values at 78, 77 and 51 corresponding to benzene ring. This aspect indicates that the thermal decomposition mechanism of the network structures follows two simultaneous paths. One path consists of the PVF-1 backbones decomposition. The other path implies the thermal decomposition of the crosslinks by urethane bond scission, decarboxylation with carbamates intermediates, release of ammonia with furan derivatives and aromatic intermediates evolvement. The higher molecular mass solid structures formed during the former stage of thermal decomposition of the networks further decompose in the latter stage following a more complex decomposition mechanism by random cleavage.

### *FTIR analysis of the evolved gases*

The FTIR spectra confirmed the MS spectra results. Figure 7 shows the FTIR spectra of the main gases evolved during thermal decomposition of PVF-1 (Fig. 7a) and NPVF-2 (Fig. 7b).

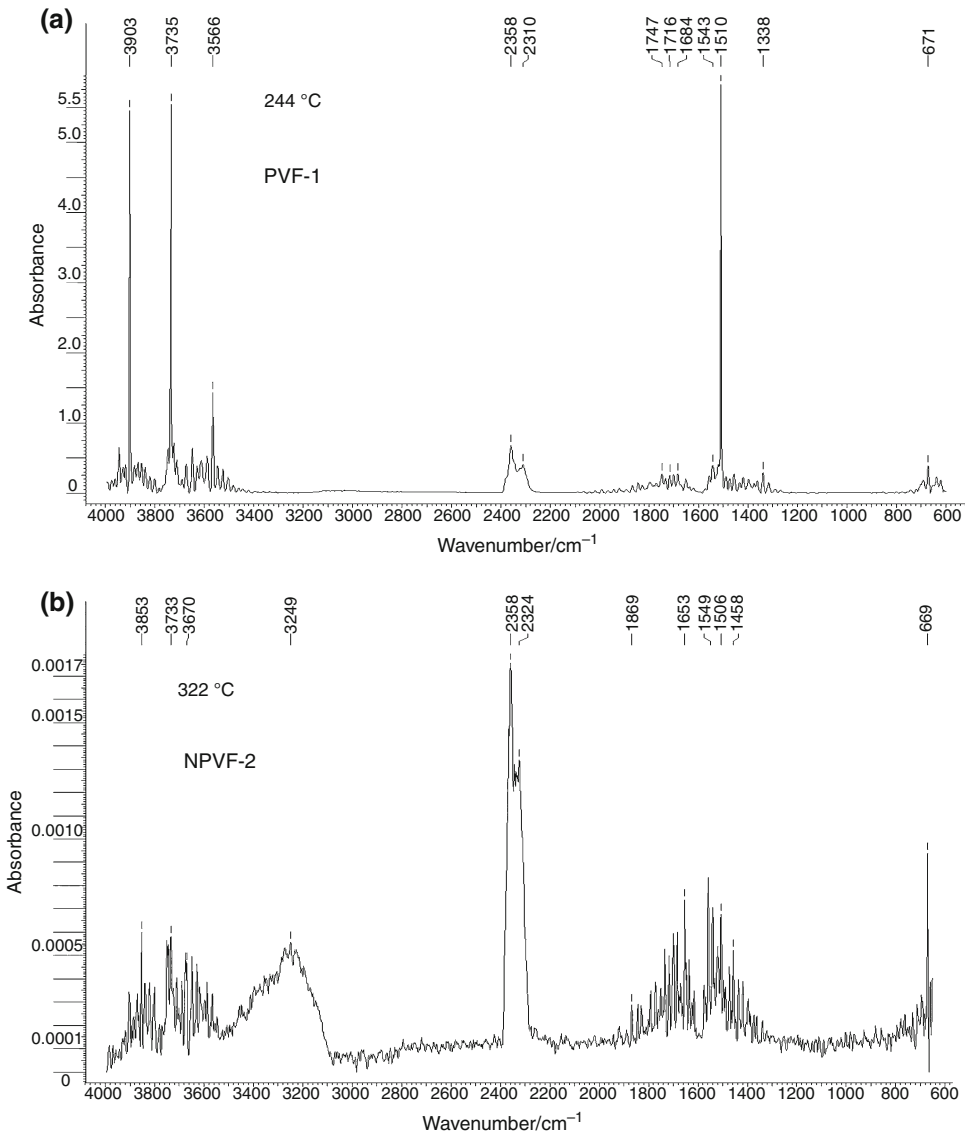


**Fig. 7** FTIR spectra of the gases evolved during the first stage of thermal decomposition of **a** PVF-1 and **b** NPVF-2

For PVF-1 (Fig. 7a), the absorption bands characteristic to carbon dioxide appear at 2,358 and 671 $cm^{-1}$. In addition, there could be observed weak absorption bands at 3,735 and 1,510 $cm^{-1}$, which are specific to water and they may appear principally due to PVF chains dehydration. The peak at 1,510 $cm^{-1}$ may also correspond to C=C stretching vibration from furan/and or polyene moieties together with the peak at 1,543 $cm^{-1}$. Among these bands, there are present peaks at 1,747 and 3,566 $cm^{-1}$ that can be attributed to the stretching vibrations of C=O and OH groups from acetic acid. For NPVF-2 (Fig. 7b), the absorption bands characteristic to carbon dioxide appear at 2,358 and 669 $cm^{-1}$. The broad peak at 3,249 $cm^{-1}$ and the regions from 1,300 $cm^{-1}$ to around 2,000 $cm^{-1}$ and 3,500–4,000 $cm^{-1}$ were attributed to the loss of water vapours. The peaks from 1,600 to 2,000 $cm^{-1}$ region represent vibrations of C=O and C=C bands, from polyenes, overlapping with those from water loss [47]. The region from 600 to 800 $cm^{-1}$ corresponds to aromatic entities evolvement.

## Thermoreversibility by DSC

The thermoreversibility of the networks has been investigated by applying multiple heating–cooling cycles in DSC (Fig. 8).

On the first heating curve of NPVF-7 (h1), one can observe the appearance of the endothermic peak characteristic to the retrodienic reaction which indicates the scission of DA cycloadduct's linkages and the recovery of PVF and bismaleimide [48]. When cooling the sample from 180 to 40 °C, there can be observed on the recorded curve (c1) the appearance of a broad exothermic peak, with

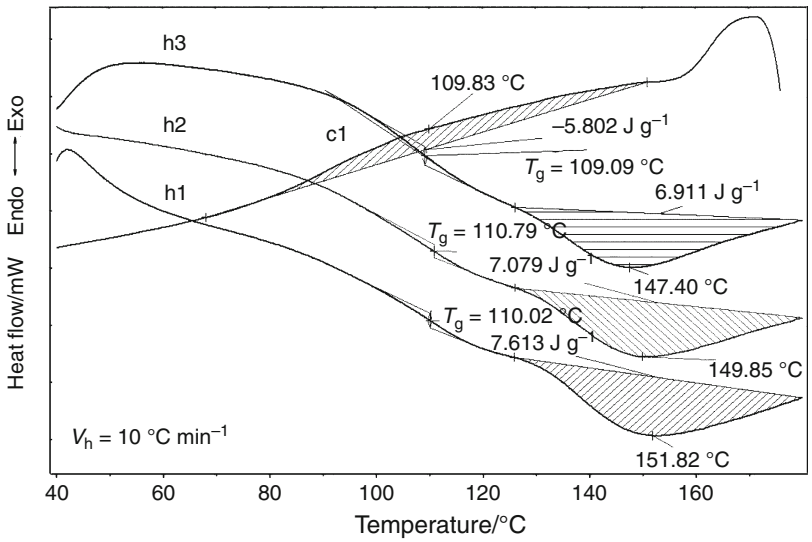


**Fig. 8** DSC heating curves of sample NPVF-7: (*h1*) first heating curve, (*h2*) second heating curve, (*h3*) third heating curve and (*c1*) cooling curve

a maximum at 110 °C, peak which suggests the re-bonding of the furan–maleimide cycloadduct by the DA reaction of these functional groups. The second (h2) and the third (h3) heating curves show a good reproducibility of the retro-dienic process, thus demonstrating the thermoreversible character of the sample.

The synthesized networks are not soluble in the same organic solvents in which the comprising compounds (PVF, BMI) are and they swell in such solvents. This issue was resolved by heating the networks in an aprotic dipolar solvent, such as *N*-methyl-2-pyrrolidone (NMP), at 160 °C for 1 h, after which they solubilized. As an exemplification, a solution 5 % of NPVF-7 in NMP was formed by the rDA reaction after maintaining it at 160 °C for 1 h (Fig. 9a). The solution turned into gel after maintaining it at 80 °C for 3 h (Fig. 9b).

## Contact angle measurements

The dynamic contact angles of PVF-1 and networks have been determined by Wilhelmy plate technique. The values for advancing ($\theta_{adv}$) and receding ($\theta_{rec}$) contact angles were obtained by measurements made in water and ethylene glycol. It was observed that both advancing and receding dynamic contact angles increase when increasing the molecular mass of PTMEG from the structure of the bismaleimide used in the synthesis. This behaviour is normal, since the hydrophobic nature of PTMEG is already known. The differences between the advancing contact angles and the receding ones, known as contact angle hysteresis, yield measures of the heterogeneity and roughness of the surface, which were also calculated (Table 2). The obtained values suggest that the surfaces of the networks' films are more homogenous than the surface of the initial PVF.

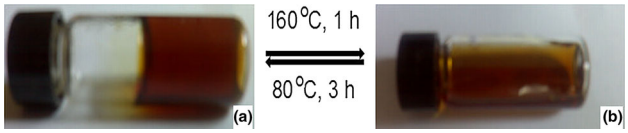


**Fig. 9** Thermally reversible behaviour of NPVF-7

The advancing dynamic contact angle values were used to calculate the free surface energy, described in Owens and Wendt's equations by the dispersive and the polar component (Eq. (1)), where $\theta$ represents the advancing dynamic contact angle, $\gamma_L$ is the free surface energy value of the liquid, $\gamma_L^d$ and $\gamma_L^p$ are the dispersive and the polar components of the free surface energy of the liquid, and $\gamma_S^p$ and $\gamma_S^d$ are the dispersive and polar components of the free surface energy of the sample's film.

$$(1+\cos\theta)\cdot\gamma_L = 2\cdot(\gamma_S^d\cdot\gamma_L^d)^{1/2} + 2\cdot(\gamma_S^p+\gamma_L^p)^{1/2}. \quad (1)$$

Using the advancing dynamic contact angles of the surface of the polymer film in two liquids (water and ethylene glycol), a two equation system was obtained and from it, the two components of the free surface energy were calculated. The increase of the molecular mass of PTMEG from the bismaleimide used in the synthesis leads to a decrease of the free surface energy of the polymer networks films. In all the cases, the polar component was higher than the dispersive one. This permitted to conclude that the dipolar forces and hydrogen bonds had an important effect in the structure of the investigated polymer films [49].

## Dynamic water vapour sorption measurements

Before sorption measurements, the samples were dried at 25 °C, in flowing nitrogen (250 mL $min^{-1}$) until the mass of the samples was in equilibrium at RH < 1 %. After this

**Table 2** Contact angle measurements

| Sample | Dynamic contact angle | | | | Hysteresis | Free surface energy | | |
|---|---|---|---|---|---|---|---|---|
| | Water | | Ethylene glycol | | | | | |
| | $\theta^{a}_{adv}$ | $\theta^{b}_{rec}$ | $\theta_{adv}$ | $\theta_{rec}$ | | $\gamma^{d}$ | $\gamma^{p}$ | $\gamma$ |
| PVF-2 | 64.89 | 36.77 | 53.61 | 21.43 | 32.12 | 6.65 | 29.82 | 36.47 |
| NPVF-3 | 76.69 | 53.58 | 67.04 | 36.99 | 23.11 | 5.66 | 22.23 | 27.9 |
| NPVF-4 | 82.9 | 57.61 | 78.62 | 38.66 | 25.29 | 2.21 | 22.6 | 24.81 |
| NPVF-5 | 84.82 | 58.8 | 79.17 | 43.48 | 26.02 | 2.86 | 19.82 | 22.68 |
| NPVF-6 | 82.16 | 56.55 | 79.06 | 39.15 | 25.61 | 1.7 | 24.4 | 26.1 |

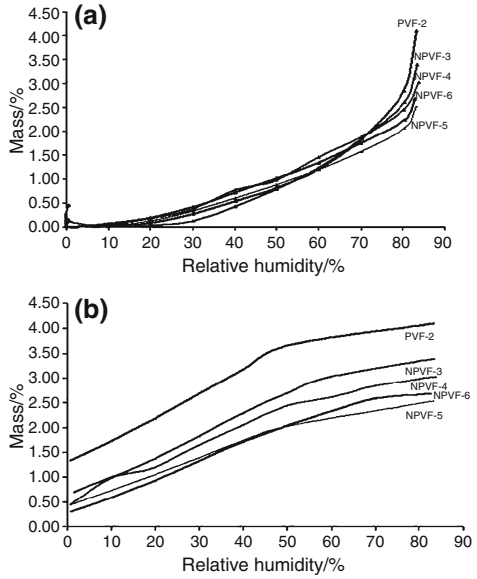


**Fig. 10** Sorption (**a**) and desorption (**b**) isotherms of the studied structures recorded at 25 °C

step, the relative humidity (RH) was gradually increased from 0 to 90 %, in 10 % humidity steps, having a pre-established equilibrium time between 10 and 20 min, and the sorption equilibrium was obtained for each one. Then, the RH decreased and the desorption curves were recorded.

Dynamic water vapour sorption is another interesting surface property of materials. In this case, the forces involved in the process vary from strong like hydrogen bonds to weak van der Waals. Sorption isotherms at 25 °C for the samples are presented in Fig. 10a and desorption ones in Fig. 10b.

The shapes of sorption/desorption isotherms are determined by the adsorption mechanism and can be explained by the nature of adsorption. Due to the presence of the hysteresis loop and according to IUPAC classification, the sorption/desorption isotherms can be associated to type **V** curves describing sorption on hydrophobic/low hydrophilic materials with weak sorbent–water interactions, with low sorption at low *RH*, and sometimes moderate sorption

**Table 3** Estimated values of the BET models parameters

| Sample | Mass/% (% dry basis) | BET analysis | |
|---|---|---|---|
| | | $A_{BET}/m^2\ g^{-1}$ | Monolayer/g $g^{-1}$ |
| PVF-2 | 4.0970 | 70.758 | 0.0202 |
| NPVF-3 | 3.3863 | 51.806 | 0.0148 |
| NPVF-4 | 3.0286 | 44.624 | 0.0127 |
| NPVF-5 | 2.5290 | 41.322 | 0.0118 |
| NPVF-6 | 2.6814 | 43.975 | 0.0125 |

at the middle RH and suddenly high water sorption at RH close to 90 [50]. The samples do not absorb or adsorb small amounts of water at low RH until the sorption capacity increases suddenly; this high water sorption results from water clusters formation followed by creation of water monolayer covering the surface at medium RH. As it can be seen, the samples have low affinity for water, the reduced water sorption onto the dry surfaces of the films confirming the structures non-polar nature. The presence of hysteresis is caused by the small rate of desorption compared with the rate of sorption and indicates that the samples possess pores.

The values of water vapour sorption capacities (sorption water measured in % dry basis) for the samples are affected by the molecular mass of PTMEG, decreasing from 4.09 to 2.52 with the increase of the molecular mass from 250 to 2,000 (Table 3). PTMEG generally exhibits low surface energy, a poor wettability and weak adhesive bonding. It absorbs very few water molecules, mainly because of its hydrophobic nature.

It can be observed from Fig. 10b that the final mass is not the same with the initial one, because a part of sorbed water remains in the sample bounded through hydrogen bonds. When water in vapour form is absorbed into the polymer, water molecules fill the voids that are formed between polymer chains. A part of this water remains trapped in the material bounded by hydrogen bonds. From the desorption branch of the isotherms and using the BET (Brunauer–Emmett–Teller) kinetic model, the BET surface

area and the value of the monolayer were calculated using the instrument's software (Table 3). The BET model is often used for modelling of the sorption isotherms and it is based on following BET equation, where $W$ is the mass of sorbed water, $W_m$ is the mass of water forming a monolayer, $C$ is a sorption constant and $RH$ is relative humidity.

$$W = \frac{W_m \cdot C \cdot \mathrm{RH}}{(1 - \mathrm{RH}) \cdot (1 - \mathrm{RH} + C \cdot \mathrm{RH})}. \quad (2)$$

This model describes the sorption isotherms up to a relative humidity of 40 %, depending on the type of sorption isotherm and on the type of material [50].

As can be seen in Table 3, the BET surface area of the films decreases from 70.8 to 41.32 ($m^2\ g^{-1}$) and the value of the monolayer from 0.0202 to 0.0118 with the increase of the PTMEG molecular mass. The characterization of these materials shows that they possess porous structures [51–57].

The study of water sorption in materials is important for many applications, such as in the coatings industry, food industry and many others.

## Conclusions

Thermoreversible networks were obtained by the DA cycloaddition reaction of PVF with urethane bismaleimides containing polyether chains, where PVF was prepared by acetalisation of PVA in DMSO as solvent and in the presence of *p*-TSA. The formation of the networks was evidenced by ATR–FTIR. The materials thermal properties were investigated using DSC and TG–FTIR–MS coupling. The thermoreversibility of the networks was demonstrated by the reproduction of the endothermic peak characteristic to the rDA process on the DSC heating curves and also the appearance of the exothermic peak, due to the DA reaction, on the DSC cooling curve. Pyrolysis behaviour was studied under nitrogen atmosphere. A thermal decomposition mechanism of the networks and PVF was discussed through evolved gas analysis. The dynamic contact angle and free surface energy values of the networks were determined. Measures of the heterogeneity and roughness of the surfaces indicated that the surfaces of the networks' films were more homogenous than the initial PVF surface. Dynamic water vapour sorption studies were also conducted. It was found that the values of water vapour sorption capacities for the samples were affected by the increasing of molecular mass of PTMEG.

**Acknowledgements** Two of the authors (C-D.V. and D.R.) acknowledge the financial support of a grant of the Romanian National Authority for Scientific Research, CNCS-UEFISCDI, Project Number PN-II-ID-PCE-2011-3-0187.

## References

1. Anbarasan R, Pandiarajaguru R, Prabhu R, Dhanalakshmi V, Jayalakshmi A, Dhanalakshmi B, Ulfath Nisha S, Gandhi S, Jayalakshmi T. Synthesis, characterizations, and mechanical properties of structurally modified poly(vinyl alcohol). J Appl Polym Sci. 2010;117:2059–68.
2. Park JS, Park JW, Ruckenstein E. On the viscoelastic properties of poly(vinyl alcohol) and chemically crosslinked poly(vinyl alcohol). J Appl Polym Sci. 2001;82:1816–23.
3. Giménez V, Mantecón A, Cádiz V. Modification of poly(vinyl alcohol) with acid chlorides and crosslinking with difunctional hardeners. J Appl Polym Sci Part A. 1996;34:925–34.
4. Figueiredo KCS, Alves TLM, Borges CP. Poly(vinyl alcohol) films crosslinked by glutaraldehyde under mild conditions. J Appl Polym Sci. 2009;111:3074–80.
5. Yang S, Liu G, Wang X, Song J. Electroresponsive behaviour of a sulfonated poly(vinyl alcohol) hydrogel and its application to electrodriven artificial fish. J Appl Polym Sci. 2010;117:2346–53.
6. Gousse C, Gandini A. Acetalization of polyvinyl alcohol with furfural. Eur Polym J. 1997;33:667–71.
7. Fernández MD, Fernández MJ, Hoces P. Poly(vinyl acetal)s containing electron-donor groups: synthesis in homogeneous phase and their thermal properties. React Funct Polym. 2008;68:39–56.
8. Chetri P, Dass NN. Preparation of poly(vinyl butyral) with high acetalization rate. J Appl Polym Sci. 2001;81:1182–6.
9. Eastman SA, Lesser AJ, McCarthy TJ. Quantitative poly(vinyl alcohol) modification in ionic liquids: esterification and urethanation with low surface tension producing reagents. Macromolecules. 2010;43:4584–8.
10. Cavusoglu J, Kusefoğlu SH. Oleophilic modification of poly (vinyl alcohol) films by functionalized soybean oil triglycerides. J Appl Polym Sci. 2011;119:2431–8.
11. David G, Ortega E, Chougrani K, Manseri A, Boutevin B. Grafting of phosphonate groups onto PVA by acetalyzation. evaluation of the anti-corrosive properties for the acetalyzed PVA coatings. React Funct Polym. 2011;71:599–606.
12. Sauca S, Giamberini M, Reina JA. Flame retardant phosphorous—containing polymers obtained by chemically modifying poly(vinyl alcohol). Polym Degrad Stab. 2013;98:453–63.
13. Gaina C, Ursache O, Gaina V, Buruiana E, Ionita D. Investigation on the thermal properties of new thermo-reversible networks based on poly(vinyl furfural) and multifunctional maleimide compounds. Express Polym Lett. 2012;6:129–41.
14. Sanyal A. Diels–Alder cycloaddition–cycloreversion: a powerful combo in materials design. Macromol Chem Phys. 2010;211:1417–25.
15. Hizal G, Tunca U, Sanyal A. Discrete macromolecular constructs via the Diels–Alder "Click" reaction. J Appl Polym Sci Part A. 2011;49:4103–20.
16. Atilla Tasdelen M. Diels–Alder "Click" reactions: recent applications in polymer and material science. Polym Chem. 2011;2:2133–45.
17. Zhou J, Guimard NK, Inglis AJ, Namazian M, Lin CY, Coote ML, Spyrou E, Hilf S, Schmidt FG, Barner-Kowollik C. Thermally reversible Diels–Alder-based polymerization: an experimental and theoretical assessment. Polym Chem. 2012;3:628–39.
18. Toncelli C, De Reus DC, Picchioni F, Broekhuis AA. Properties of reversible Diels–Alder furan/maleimide polymer networks as function of crosslink density. Macromol Chem Phys. 2012;213:157–65.
19. Gandini A. The furan/maleimide Diels–Alder reaction: a versatile click–unclick tool in macromolecular synthesis. Prog Polym Sci. 2013;38:1–28.

20. Gandini A, Coelho D, Silvestre AJD. Reversible click chemistry at the service of macromolecular materials. Part 1: kinetics of the Diels–Alder reaction applied to furan–maleimide model compounds and linear polymerizations. Eur Polym J. 2008;44:4029–36.
21. Kavitha AA, Singha NK. "Click chemistry" in tailor-made polymethacrylates bearing reactive furfuryl functionality: a new class of self-healing polymeric material. Appl Mater Interface. 2009;1:1427–36.
22. Ishida K, Nishiyama Y, Michimura Y, Oya N, Yoshie N. Hard–soft conversion in network polymers: effect of molecular weight of crystallizable prepolymer. Macromolecules. 2010;43:1011–5.
23. Ishida K, Weibel V, Yoshie N. Substituent effect on structure and physical properties of semicrystalline Diels–Alder network polymers. Polymer. 2011;52:2877–82.
24. Aumsuwan N, Urban MW. Reversible releasing of arms from star morphology polymers. Polymer. 2009;59:33–6.
25. Swanson JP, Rozvadovsky S, Seppala JE, Mackay ME, Jensen RE, Costanzo PJ. Development of polymeric phase change materials on the basis of Diels–Alder chemistry. Macromolecules. 2010;43:6135–41.
26. Scheltjens G, Brancart J, De Graeve I, Van Mele B, Terryn H, Van Assche G. Self-healing property characterization of reversible thermoset coatings. J Therm Anal Calorim. 2011;105:805–9.
27. Marref M, Mignard N, Jegat C, Taha M, Belbachir M, Meghabar R. Epoxy-amine based thermoresponsive networks designed by Diels–Alder reactions. Polym Int. 2013;62:87–98.
28. Wei HL, Yang Z, Chen Y, Chu HJ, Zhu J, Li ZC. Characterisation of *N*-vinyl-2-pyrrolidone-based hydrogels prepared by a Diels–Alder click reaction in water. Eur Polym J. 2010;46:1032–9.
29. Wei HL, Yang J, Chu HJ, Yang Z, Ma CC, Yao K. Diels–Alder reaction in water for the straightforward preparation of thermoresponsive hydrogels. J Appl Polym Sci. 2011;120:974–80.
30. Mcelhanon JR, Russick EM, Wheeler DR, Loy DA, Aubert JH. Removable foams based on an epoxy resin incorporating reversible Diels–Alder adducts. J Appl Polym Sci. 2002;85:1496–502.
31. James HA. Thermally removable epoxy adhesives incorporating thermally reversible Diels–Alder adducts. J Adhesion. 2003;79:609–16.
32. Defize T, Riva R, Thomassin JM, Jérôme C, Alexandre M. Thermo-reversible reactions for the preparation of smart materials: recyclable covalently-crosslinked shape memory polymers. Macromol Symp. 2011;309–310:154–61.
33. Defize T, Riva R, Jérôme C, Alexandre M. Multifunctional poly(ε-caprolactone)-forming networks by Diels–Alder cycloaddition: effect of the adduct on the shape-memory properties. Macromol Chem Phys. 2012;213:187–97.
34. Kavitha AA, Singha NK. A tailor-made polymethacrylate bearing a reactive diene in reversible Diels–Alder reaction. J Polym Sci Part A. 2007;45:4441–9.
35. Kavitha AA, Singha NK. Atom-transfer radical copolymerization of furfuryl methacrylate (FMA) and methyl methacrylate (MMA): a thermally-amendable copolymer. Macromol Chem Phys. 2007;208:2569–77.
36. Goiti E, Heatley F, Huglin MB, Rego JM. Kinetic aspects of the Diels–Alder reaction between poly(styrene-*co*-furfuryl methacrylate) and bismaleimide. Eur Polym J. 2004;40:1451–60.
37. Liu YL, Chen YW. Thermally reversible cross-linked polyamides with high toughness and self-repairing ability from maleimide- and furan-functionalized aromatic polyamides. Macromol Chem Phys. 2007;208:224–32.
38. Liu YL, Hsieh CY, Chen YW. Thermally reversible cross-linked polyamides and thermo-responsive gels by means of Diels–Alder reaction. Polymer. 2006;47:2581–6.
39. Gaina C, Ursache O, Gaina V, Varganici CD. Thermally reversible cross-linked poly(ether–urethane)s. Express Polym Lett. 2013;7:636–50.
40. Okhay N, Mignard N, Jegat C, Taha M. Diels–Alder thermoresponsive networks based on high maleimide–functionalized urethane prepolymers. Des Monom Polym. 2013;16:475–87.
41. Varganici CD, Ursache O, Gaina C, Gaina V, Rosu D, Simionescu BC. Synthesis and characterization of a new thermoreversible polyurethane network. Ind Eng Chem Res. 2013;52:5287–95.
42. Gaina C, Ursache O, Gaina V, Buruiana E. Novel thermally reversible epoxy–urethane networks. Des Monom Polym. 2012;15:63–73.
43. Varganici CD, Paduraru OM, Rosu L, Rosu D, Simionescu BC. Thermal stability of some cryogels based on poly(vinyl alcohol) and cellulose. J Anal Appl Pyrol. 2013;104:77–83.
44. Shaulov AY, Lomakin SM, Zarkhina TS, Rakhimkulov AD, Shilkina NG, Muravlev YB, Berlin AA. Carbonization of poly(vinyl alcohol) in blends with boron polyoxide. Phys Chem. 2005;403:772–6.
45. Rosu D, Tudorachi N, Rosu L. Investigations on the thermal stability of a MDI based polyurethane elastomer. J Anal Appl Pyrol. 2010;89:152–8.
46. Patel P, Hull TR, McCabe RW, Flath D, Grasmeder J, Percy M. Mechanism of thermal decomposition of poly(ether ether ketone) (PEEK) from a review of decomposition studies. Polym Degrad Stab. 2010;95:709–18.
47. Varganici CD, Durdureanu-Angheluta A, Rosu D, Pinteala M, Simionescu BC. Thermal degradation of magnetite nanoparticles with hydrophilic shell. J Anal Appl Pyrol. 2012;96:63–8.
48. Varganici CD, Ursache O, Gaina C, Gaina V, Simionescu BC. Studies on new hybrid materials prepared by both Diels–Alder and Michael addition reactions. J Therm Anal Calorim. 2013;111(2):1561–70.
49. Hamciuc E, Hamciuc C, Cazacu M. Comparative evaluation of some properties of two poly(ether-imide) thin films with/without fluorine in the structure. Rev Roum Chim. 2009;54:1007–13.
50. Ng EP, Mintova S. Nanoporous materials with enhanced hydrophilicity and high water sorption capacity. Microporous Mesoporous Mater. 2008;114:1–26.
51. Brunauer S, Deming LS, Deming WE, Teller E. On a theory of the van der Waals adsorption of gases. J Am Chem Soc. 1940;62:1723–32.
52. Bankauskaite A, Baltakys K, Mezinskis G. Modified hydrotalcites application as precursors for (Na, K)Mg/Al spinel-type compounds formation. J Therm Anal Calorim. 2014;. doi:10.1007/s10973-014-3737-z.
53. Rangel-Rivera P, Rangel-Porras G, Pfeiffer-Perea H, Lima-Muñoz E. Thermoanalytical study of acid-treated clay containing amino acid immobilized on its surface. J Therm Anal Calorim. 2014;115:1359–69.
54. Charmas B. Adsorption and calorimetric studies of hydrothermally modified carbosils. J Therm Anal Calorim. 2014;115:1395–405.
55. Athanasiou A, Mitsionis A, Skouras G, Todorova N, Trapalis C, Vaimakis T. Thermogravimetric study of the surfactant–diethanolamine–titanium isopropoxide system behavior. J Therm Anal Calorim. 2014;116:15–25.
56. Ledesma B, Román S, Álvarez-Murillo A, Sabio E, González–García CM. Fundamental study on the thermal regeneration stages of exhausted activated carbons: kinetics. J Therm Anal Calorim. 2014;115:537–43.
57. Staszczuk P, Rycyk M. Studies of adsorption and total heterogeneity properties of pure and modified carbon nanotube surfaces. J Therm Anal Calorim. 2013;114:1125–33.